NASA Technical Memorandum 79085

CHARACTERISTICS OF AEROELASTIC INSTABILITIES IN TURBOMACHINERY - NASA FULL SCALE ENGINE TEST RESULTS

Joseph F. Lubomski
Lewis Research Center
Cleveland, Ohio

TECHNICAL PAPER to be presented at the
Fourth International Symposium
on Air Breathing Engines
sponsored by the American Institute
of Aeronautics and Astronautics
Lake Buena Vista, Florida, April 1-6, 1979

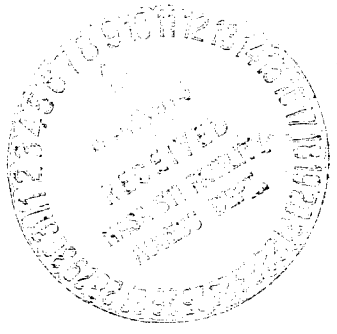

1. Report No.	2. Government Accession No.	3. Recipient's Catalog No.
NASA TM-79085		

4. Title and Subtitle	5. Report Date
CHARACTERISTICS OF AEROELASTIC INSTABILITIES IN TURBOMACHINERY - NASA FULL SCALE ENGINE TEST RESULTS	6. Performing Organization Code

7. Author(s)	8. Performing Organization Report No.
Joseph F. Lubomski	E-9908
	10. Work Unit No.

9. Performing Organization Name and Address	11. Contract or Grant No.
National Aeronautics and Space Administration Lewis Research Center Cleveland, Ohio 44135	
	13. Type of Report and Period Covered
12. Sponsoring Agency Name and Address	Technical Memorandum
National Aeronautics and Space Administration Washington, D.C. 20546	14. Sponsoring Agency Code

15. Supplementary Notes

16. Abstract

Several aeromechanical programs have been conducted in the NASA/USAF Joint Engine System Research Programs. The scope of these programs, the instrumentation, data acquisition and reduction, and the test results are discussed. Data pertinent to four different instabilities were acquired; two types of stall flutter, choke flutter and a system mode instability. The data indicates that each instability has its own unique characteristics. These characteristics are described.

17. Key Words (Suggested by Author(s))	18. Distribution Statement
Turbofan; Turbojet; Turbomachine blades; Aeroelasticity; Subsonic flutter; Engine tests; Altitude tests; Full scale tests	Unclassified - unlimited STAR Category 39

19. Security Classif. (of this report)	20. Security Classif. (of this page)	21. No. of Pages	22. Price*
Unclassified	Unclassified		

* For sale by the National Technical Information Service, Springfield, Virginia 22161

CHARACTERISTICS OF AEROELASTIC INSTABILITIES IN TURBOMACHINERY - NASA FULL SCALE ENGINE TEST RESULTS

Joseph F. Lubomski
NASA-Lewis Research Center
Cleveland, Ohio

Abstract

Several aeromechanical programs have been conducted in the NASA/USAF Joint Engine System Research Programs. The scope of these programs, the instrumentation, data acquisition and reduction, and the test results are discussed. Data pertinent to four different instabilities were acquired; two types of stall flutter, choke flutter and a system mode instability. The data indicates that each instability has its own unique characteristics. These characteristics are described.

E-9908

Nomenclature

C_1	negative damping coefficient
C_2	positive damping coefficient
G	shear modulus of elasticity
I_o	mass moment of inertia
J	polar area moment of inertia
ε	constant in Van der Pol's equation
ζ	damping coefficient
θ	dimensionless angular displacement
θ	angular displacement
ω_f	frequency of unstable motion
ω_n	natural frequency of blade or vane

Introduction

Problems due to aeroelastic instabilities have occurred in recent development engines that have resulted in costly and time-consuming program delays. These have provided an impetus throughout industry and government to develop a better understanding of the nature of aeroelastic instabilities and to evolve design tools to avoid such problems. The NASA and the USAF have several joint programs in this effort. One of these is the Joint Engine System Research Programs, the objective of which is to investigate technology areas of mutual interest, one of which is aeroelastic instabilities.

In the Joint Engine System Research Programs a thoroughly instrumented engine is installed in an altitude facility and tested at simulated flight conditions. For the aeromechanical programs the flight conditions selected were those at which aeroelastic instabilities were known to exist based on engine development histories. Instabilities were induced at these test conditions and a comprehensive set of aerodynamic and aeromechanical data were obtained prior to entering and during the instability regions. This data is now a part of a data bank available to help understand aeroelastic phenomena and for use in developing and verifying design tools. This data has been validated and does define the behavior of aeroelastic instabilities in an engine at flight conditions.

To date two sets of aeromechanical tests have been completed. Data relative to stall flutter, choke flutter and a system mode instability has been collected. This was accomplished using two different engines, an afterburning turbofan engine and an afterburning turbo-jet engine. Both engines are high thrust to weight ratio, high performance engines representative of current technology.

This paper will outline the scope of these two test programs, the test procedures and instrumentation used, the data acquisition and reduction methods used, and the test results.

Types of Aeroelastic Instabilities

An aeroelastic instability is a self-excited vibration of an airfoil, single or cascaded, whereby the unstable motion is generated and sustained due to the unique motion of the airfoil in the airstream. Thus the oscillating airfoil is extracting energy from the airstream and is aerodynamically negatively damped.

Aeroelastic instabilities in turbomachinery are generally now classified as being one of five distinct types[1] relative to the location of the instability on a compressor map such as shown in Fig. 1. These are as follow:

I. Subsonic/transonic stall flutter.
II. Choke flutter.
III. Low back pressure supersonic flutter.
IV. High back pressure supersonic flutter.
V. Supersonic stall flutter.

All of these instabilities are being investigated in current NASA/USAF programs. However, in the Joint Engine System Research Programs to date, no supersonic instabilities have been encountered, thus the discussions to follow will be limited to subsonic/transonic stall flutter and choke flutter with one exception. This exception is a system mode instability relative to which only a limited amount of data has been acquired thus making it inappropriate at this time to attempt to classify it unequivocally into one of these types.

Subsonic/transonic stall flutter was historically the most commonly found aeroelastic instability in turbomachinery prior to the development of high tip speed fans operating supersonically at the tip. It occurs near the stall line at large angles of incidence and is accompanied by flow separation for part of or all of the oscillatory cycle. The flutter frequency is near but not necessarily equal to one of the airfoil natural frequencies in one of the first three fundamental modes, viz; first bending, first torsion or second bending.

Choke flutter occurs near the choke line at small positive or negative incidence angles and is accompanied by choking in the cascaded blade passage. The flutter frequency is again near but not necessarily equal to a blade natural frequency, usually first bending. In earlier engines choke flutter usually affected turbine stages rather

than compressor stages and is still a problem on high aspect, low pressure steam turbines.

A system mode instability[2] will normally afflict a shrouded blade rotor assembly. Instabilities of this type are dependent on shroud coupling and occasionally disk coupling. They are characterized by flutter frequencies not necessarily associated with a fundamental blade frequency and the blade vibratory mode shape is more often than not a coupled mode, such as a coupling of first bending and first torsion. This type of instability has not been thoroughly documented.

Apparatus

The two series of tests completed to date were conducted using two different types of engines. The first series of tests were done using a twin spool, high performance, afterburning turbofan engine which had a history of an aeroelastic instability with a preproduction first stage fan. The installation of this engine in the test facility is shown in Fig. 2. This engine has a three stage fan as shown in Fig. 3. The fan blades have part span shrouds and are made of titanium. The bypass airflow ratio is nominally 0.7 to 1 at sea level static standard day conditions. The diameter at the fan inlet is nominally 88.34 cm (34.78 in.). This engine was susceptible to subsonic/transonic stall flutter in above shroud torsion at elevated inlet temperatures and pressures i.e. at high Mach number flight conditions. This particular engine was tested in the PSL-1 altitude chamber of the Lewis Propulsion System Laboratory.

The second engine tested was a single spool afterburning turbojet. The installation of this engine in the test facility is shown in Fig. 4. This engine has a 9 stage titanium bladed compressor as shown in Fig. 5. The first two stages have part span shrouds. The inlet guide vanes and the first three stators are variable. The inlet diameter of this engine is 43.61 cm (17.17 in.). This engine was tested in the PSL-2 altitude chamber of the Lewis Propulsion Systems Laboratory. This engine had development problems with several types of instabilities. The third stage and the fifth stage rotors were susceptible to choke flutter. The fifth stage rotor instabilities occurred at cold inlet temperatures, less than -20° C (-4° F). The third rotor instabilities occurred over a range of inlet temperatures bounded by 15.5° C (60° F) and 49° C (120° F) at elevated inlet pressures. The second rotor had exhibited a system mode instability at elevated inlet pressures and temperatures. The fourth stage stator had a stall flutter instability at high inlet pressures and cold inlet temperatures.

Instrumentation

Data in the aeromechanical programs were acquired using a wide variety of instrumentation and data reduction techniques. Jones, et al.,[3] comprehensively discusses the type of instrumentation and the location of this instrumentation in the engine as used in the turbofan program. The turbojet program had essentially the same types of instrumentation and used the same data acquisition and reduction techniques. As background information the aerodynamic and aeromechanical instrumentation will be summarized herein.

Aerodynamic Instrumentation

The principal measurements taken are total temperatures, total pressures and static pressures. These are obtained at all principal engine stations using a number of radial rakes. Wall static pressures are also obtained at these stations. Interstage data was also obtained using 5 element radial temperature and total pressure rakes along with two wall static pressure measurements at each location. In the turbofan program this instrumentation was mounted into the leading edge of a stator vane in each of the three fan stator stages to avoid blockage. In the turbojet program probes were designed and built that fitted in the stator rows for each of the nine stages. A number of these were strain gaged and monitored during the test program. The arrangement of the aerodynamic instrumentation by stations for the turbofan program is shown in Fig. 6. The arrangement in the turbojet program was similar.

The data obtained from this instrumentation was recorded on two systems. One system is used to record the steady-state data points and the other system is used to record transient data. In the transient system data is obtained during a transient with a sample rate of up to 150 a second. This recorded data is then processed and reduced off-line using a large scientific computer. A significant accomplishment of the aeromechanical programs was the acquisition of comprehensive aerodynamic data while an instability was occurring in the engine. Normally the instability was sustained at a predetermined safe stress level for from 1 to 2 minutes while data was being acquired on all data systems.

Aeromechanical Instrumentation

In the aeromechanical programs data was acquired using three types of instrumentation. The primary source of data was strain gages mounted on the fan and compressor blades and vanes. The data from these were used for on-line monitoring as well as for post-run analysis. In addition a photoelectric scanning (PES) system was developed[4] which used light probes. This system made it possible to observe online the nonintegral response of all the blades on a given rotor. The data from this system was also recorded as either video tape or digitized for post run analysis. A third method, developed by Kurkov[5] utilized data recorded from high response pressure transducers which when analyzed in the frequency domain proved to be useful in defining the aeromechanical modes of a rotor assembly in flutter.

Strain gages were mounted on selected blades and vanes by the engine manufacturers after bench testing the blades and vanes to determine the exact natural frequencies and mode shapes. In the turbofan program all of the fan blades were bench tested individually and as an assembly to determine the system modes. In the turbojet program only a select number of blades were bench tested due to the large number of blades and vanes in-

volved in the program. In the turbofan program the three fan rotor and stator stages were strain gaged with the bulk of the strain gages being on the first stage rotor since only it was susceptible to an aeroelastic instability. Three fan builds were made and tested and in each build there was a slight variation in the strain gage distribution. Only one build was made and tested in the turbojet program. In this build all nine stages had strain gaged rotor blades as did the last six stator stages. A 100 channel slipring was used in both programs to transmit the rotor strain gage signals thus 50 rotor strain gage signals were monitored at a time. In addition to these between 30 and 40 stator gages were monitored and recorded.

Strain gage signals are monitored in the time domain and in the frequency domain. Each strain gage signal is displayed on a small oscilloscope for continuous monitoring in the time domain. Currently up to 112 signals can be handled simultaneously. These signals can also be quickly patched into large oscilloscopes for expanded analysis in the time domain or they can be selectively patched into a number of systems for analysis in the frequency domain. In the aeromechanical programs the following systems were available and were used:

1. A software based Fast Fourier Transform (FFT) Digital Signal Analyzer which can handle two channels simultaneously.
2. Several analog spectral analyzers.
3. A microprocessor based multichannel vibration and flutter monitor[6] which can handle up to 16 channels simultaneously.

All strain gage data is recorded for post run analysis. Forty FM channels are available within the test facility for the more pertinent strain gages and 180 FM multiplexed channels are available in a central analog facility for all the strain gages. Reduction of strain gage data is done in the time domain and in the frequency domain. Time domain data reduction is done to obtain overall stress levels, waveform and event history. Frequency domain data reduction is used extensively due to the availability of several FFT systems. In the frequency domain the data is processed to obtain power spectral density, linear spectra, transfer functions and cross correlation function. The coherence function is always computed whenever time averaging is used.

Results and Discussion

Turbofan Program-Subsonic Stall Flutter

The program using the turbofan engine was conducted in three phases during which 33 data points in flutter were obtained at a variety of inlet conditions and speeds. Aerodynamic and aeromechanical flutter data were obtained at inlet pressures between 103 and 207 kPa (15 and 30 psia) and at inlet temperatures from 135° to 171° C (275° to 340° F). The flutter data was obtained at corrected fan speeds between 64 and 73 percent of design speed. The first phase of the program was conducted to develop monitoring techniques, instrumentation and operational procedures and to locate the flutter regions within the engine flight envelope. The instability region was approached by setting inlet conditions and speed. Then the nozzle was throttled while holding constant corrected speed to increase fan back pressure. Only stall flutter in above shroud torsion of the first stage fan rotor was found and documented at several conditions. The fan assembly was then removed, disassembled, instrumentation refurbished and the fan assembly rebuilt for Phase II testing. It was during the Phase II test program that the majority of the data was obtained. For the Phase III build the instrumented fan blades were removed and replaced with different instrumented blades. Using this build several of the previous test points were repeated and additional flutter data was obtained which proved to be of significance.

The response of the rotor blades in flutter was varied. At incipient flutter a low level irregular beating was observed on the strain gage signals probably due to flow separation. Upon developing full flutter the strain gage signals usually became periodic. Several flutter frequencies were observed of which one was predominant on most of the strain gages. A blade to blade variation in maximum amplitude was observed on the strain gages and on the light probes. Usually a small group of blades would respond initially upon penetrating the flutter boundary and then as the excursion into the flutter region progressed more of the blades would become active.

No unique and common interblade phase angle was observed from the strain gage data. Light probe observations indicated that a few small groups of blades may have been coupling with a common interblade phase angle but complete coupling of all the blades on the rotor assembly did not occur. The excursion into the flutter region was normally stopped when any single strain gage indicated an overall stress level of 75 percent of allowable, as specified by the engine manufacturer. A few excursions were made beyond this to see if complete coupling could be induced but were unsuccessful. Thus the flutter or aeromechanical mode appears to be mistumed as defined by Whitehead.[7]

The flutter frequency observed usually did not vary while the rotor blades were in flutter as shown in the expanded spectrum plot of Fig. 7. This data is from a strain gage located slightly above the shroud at the trailing edge. This blade is responding at 1072 Hz, which was the primary flutter frequency, with a maximum amplitude of ±50.3 MPa (±7.3 ksi) at that frequency. The response at 1040 Hz is a secondary flutter frequency from a blade fluttering at that frequency located three blades away on the rotor. This will be discussed in detail later. The response at 1120 Hz is the eighth engine order response. During the time that the rotor was in flutter these frequencies did not change and the interblade phase angle between any pair of adjacent blades remained highly coherent.

An exception to this behavior was observed at either the lower inlet pressures or inlet temperatures whenever flutter occurred. At these inlet conditions the flutter frequencies varied irregularly as did the amplitudes. This is shown in the expanded spectrum plots of Figs. 8 and 9. This data is from the same strain gage as discussed previously but for a lower inlet temper-

ature, 135° C (275° F). These data are single average FFT linear spectra taken 1 minute and 20 seconds apart during the same steady-state data point. In between this time there were no significant changes in engine parameters. These data show a number of flutter frequencies occurring one of which is common to both time frames at 1064 Hz. A frequency content such as those shown will yield an erratic beat response in the time domain commonly associated with flow separation vibrations. A deeper excursion into the flutter zone was made once to attempt to develop a unique flutter frequency but this only resulted in rotating stall which annihilated the aeroelastic instability. Time averaging this type of data in the frequency domain usually shows between 3 and 4 predominant flutter frequencies with good coherence of most of the interblade phase angles. A similar response was observed in data taken at an inlet pressure of 103 kPa (15 psia) and an inlet temprature of 171° C (340° F). Time averaging of these data yielded a poor coherence function relative to the interblade phase angles, less than 0.4, and only one predominant frequency. Thus it would appear that there exists a domain which is a function of stage inlet conditions where the flutter response is irregular and aperiodic that separates the well defined flutter domain and the flutter clear domain.

Inlet pressure and temperature besides affecting the rotor blade's response also had a significant influence on the flutter boundary location on the fan performance map. Over the range of inlet pressures and temperatures investigated in the test program it was found that increasing inlet temperature and increasing inlet pressure were both destabilizing. That is, increasing either of these parameters tended to move the instability boundary nearer the operating line. This is shown in Fig. 10 which is a segment of a fan performance map. Five data points obtained at approximately the same corrected speed from a single strain gage at nominally the same stress level are plotted showing the effect of inlet pressure and temperature on the flutter boundary.

Another aspect of varying the inlet pressure and temperature was the effect on the flutter frequency. Increasing the inlet pressure had the most significant effect. This is shown in Fig. 11 which is a plot of the flutter frequency obtained from a single strain gage mounted on the blade in position 1 on the fan rotor. Two sets of frequency data are shown. One set encompasses the frequency range between 1060 Hz and 1900 Hz which was the primary or most common flutter frequency observed on all the instrumented blades. The second set of data between 1020 Hz and 1050 Hz is a secondary flutter frequency which commonly showed up only on those blades around position 1 on the rotor. It should be noted that the behavior of the two sets of data with respect to inlet temperature and pressure is similar, thus the two sets of data are probably a common phenomena. It was found that increasing inlet pressure tended to clearly decrease the flutter frequency in what appears to be a linear function. Also increasing the inlet temperature slightly decreased the flutter frequency. This latter effect is probably due to the temperature effect on the shear modulus.

Another effect not shown but which affects this data was the effect of physical or mechanical speed. Increasing the engine speed for a given inlet temperature and pressure tended to slightly decrease the flutter frequency. As an example, two data points taken at inlet conditions of 138 kPa (20 psia), 171° C (340° F) and 700 rpm apart had a difference in flutter frequency of 4 Hz with the higher speed having the lower frequency. This was typical of all the data taken.

The functional behavior of the flutter frequency with an engine parameter may be highly significant. Aeroelastic instabilities can be considered to be a limit cycle phenomena. Den Hartog[8] developed a simple single degree of freedom model which can be analogous to the behavior of a blade in flutter. Den Hartog's model formulated as a single degree of torsion model yields the equation:

$$I_o\ddot{\theta} - (C_1 - C_2\theta^2)\dot{\theta} + GJ\theta = 0 \qquad (1)$$

where C_1 is the negative part of the damping coefficient and C_2 the positive part. As can be seen from Eq. (1) small values of θ will yield a negative damping coefficient while large values of θ will yield a positive damping coefficient. For periodic motion the sign and value of the damping coefficient will vary during a single oscillation. Proceeding with Den Hartog's development and making the variables dimensionless yields:

$$\ddot{\theta} - \varepsilon(1 - \theta^2)\dot{\theta} + \theta = 0 \qquad (2)$$

where

$$\varepsilon = C_1/I_o\omega_n \qquad (3)$$

Eq. (2) is a common form of Van der Pol's equation which defines the behavior of a nonlinear, self-excited relaxation oscillation. The period for a relaxation oscillation is $2\varepsilon/\omega_n$ or

$$\omega_f = \frac{\omega_n}{2\varepsilon} \qquad (4)$$

Thus as ε increases with ω_n remaining constant the frequency of the relaxation oscillation will decrease. The Van der Pol coefficient ε will increase, holding I_o and ω_n constant only if the negative part of the damping coefficient, C_1, increases.

Applying this development to the flutter frequency data it can be hypothesized that the change in flutter frequency with increasing inlet pressure may be due to the effect of the stage inlet pressure on the negative work done during an oscillatory cycle. The small change in flutter frequency due to the inlet temperature is probably due to the change in natural frequency (ω_n) because of change in structural stiffness as a result of temperature. In a similar manner increasing rotor speed tends to decrease the torsional natural frequency, thus reducing the flutter frequency, which is consistent with data observations.

The effect of changing the instrumented blades and repeating several data points yielded

several interesting results. The secondary flutter frequency (1020 to 1050 Hz) did not appear. The location of the maximum response on the rotor as observed with light probes shifted by about 100°. That is the aeromechanical mode of the rotor changed, but still remained mistuned. In conjunction with this the flutter boundary on the fan performance map, as established by the strain gage on the blade in position 1, moved closer to the operating line. That is, in Phase III for the same conditions flutter initiated at a lower pressure ratio than that observed in Phase II. The pressure ratio at which flutter was found in Phase III was approximately 3 percent lower than in Phase II. The flutter frequencies were essentially the same varying only by about 3 Hz.

The disappearance of the secondary flutter frequency may be a result of changing an instrumented blade near position 1. It should be noted that none of the strain gages on this blade were functional making it impossible to verify the supposition being made. This blade had a room temperature bench test natural frequency of 1045 Hz, the lowest of all the blades in the rotor assembly and thus making it a likely candidate to be susceptible to stall flutter. It was replaced by a blade with a much higher torsional natural frequency. The change in aeromechanical mode and the apparent decrease in stall flutter margin cannot be readily explained. The most responsive blades in Phase II, and the most responsive blade in Phase III, were common to both phases. It may be conjectured that in making the rotor build for Phase III build up tolerances may have changed sufficiently to make different blades more susceptible to flutter as for example an incidence change.

The concept of establishing a flutter boundary on a fan performance map using either a single or a few strain gages is an arbitrary procedure. Mistuned flutter modes are common in an engine and one does not know that the instrumented blade being used is the most responsive in any one flutter mode. Thus the changes in flutter boundary noted herein should not be judged quantitatively.

Turbojet Program-Choke Flutter

The majority of the data obtained in the turbojet aeromechanical program involved the choke flutter phenomena. Thirty one data points at a variety of inlet conditions and speeds were obtained documenting this phenomena as it affected the third stage rotor. This instability occurred in the first bending mode. Comprehensive aerodynamic and aeromechanical flutter data were obtained at inlet pressures between 103 and 200 kPa (15 and 29 psia) with inlet temperatures between 15.5° C and 49° C (60° and 120° F). The instability occurred at corrected speeds between 95 and 103 percent of design speed. In order to induce the instability it was necessary to off-schedule the compressor variable geometry since the operational configuration of the engine was free of this instability. Flutter data was obtained with the first stator opened off-schedule 4.4° and also with the second stator closed off-schedule 2° and 4.3°. Only one stator was off-schedule at any one time. Opening stator 1 allows an increase in mass flow which tends to slightly decrease the incidence on rotor 3 while closing stator 2 directly decreases the incidence on rotor 3.

The response of the rotor blades to the instability was quite different from the stall flutter response discussed previously. All of the strain gaged blades responsed at the same flutter frequency but with varying blade to blade maximum amplitudes. The instability was approached by doing a slow acceleration up along the operating line and flutter came in softly. That is, the stress levels built up gradually and were controlled. There was no warning of incipient flutter as there is with stall flutter as characterized by the erratic beat phenomena. There was a regular steady beat more often than not as the instability developed which persisted as the instability grew. This was due to the presence of an engine order response in close proximity to the flutter frequency as seen in the spectrum plot of Fig. 12. This spectrum is typical of all the data obtained. Common to all the data analyzed was the coexistence of a blade engine order resonant response with the flutter response. The instability frequency varied with speed, inlet pressure and inlet temperature but at no time did it vary more than 5 percent from an engine order. At times it was higher, at times lower, and occasionally was coincident with an engine order. This is quite unlike stall flutter. A stall flutter response has been observed to occur at an engine order frequency but more often than not the flutter frequency will be well removed from an engine order response frequency and will be independent of it.

The effect of increasing either inlet temperature or inlet pressure was found to be destabilizing. If either one or both of these were increased the instability would occur at a lower corrected speed. This can be seen in Fig. 13 which is a plot of flutter data points as a function of inlet temperature versus mechanical speed and corrected speed. From this figure we can see that increasing inlet pressure is destabilizing as is increasing inlet temperature with respect to corrected speed but not with respect to physical speed. Decreasing incidence was found to be destabilizing as seen from the two sets of data shown. With the second stator closed the incidence angle will be smaller than that with the first stator open.

An indication of choke flutter was obtained while accelerating the engine. As this is done the overall compressor pressure ratio increases. However, it was observed from the third rotor aerodynamic stage data that the stage pressure ratio was decreasing as the engine was accelerated indicating stage choking. This was observed to occur much sooner than any strain gage activity.

The effect of inlet temperature and inlet pressure on the flutter frequency is shown in Fig. 14. Here we see that the flutter frequency decreases as the pressure increases or as the temperature decreases. This is indicative of a density effect on the flutter frequency. Assuming that choke flutter is an instability such as a relaxation limit cycle amenable to definition by an equation of the Van der Pol type it can then be assumed that the negative work during an oscillatory cycle is a function of the air density. Also in evidence in Fig. 14 is an indication of a

change in aeromechanical mode of four of the flutter data points. For these four points the most responsive blade was different from the other ten data points. The phenomena of mode shape changes has also been observed in the stall flutter data on one occasion but at that time it was attributed to an unintentional bleed from a video view port. No explanation has been found for the change in the turbojet data.

Turbojet Program - Stall Flutter

Prior to the turbojet aeromechanical program an aerodynamic program was conducted using the same model of engine. In this program the stators were strain gaged and monitored. During a part of this program while acquiring research data a fourth stator vane instability was encountered unexpectedly. While taking data at 105.5 percent of corrected design speed at inlet conditions of 138 kPa (20 psia) and -29° C (-20° F), some action was observed on the fourth stators that was due to either buffeting or flow separation. At 106 percent corrected speed an instability developed in the second bending mode. Since there was no previous documentation on this instability its investigation was included in the aeromechanical program. Ten data points were obtained, all above 104 percent corrected design speed and at inlet conditions from 138 kPa to 200 kPa (20 to 29 psia) and -29° to 2° C (-20° to 35° F).

Only two strain gages were functional for all of the data points obtained, thus the strain gage data is somewhat limited. For all but one data point the flutter frequency was the same on both strain gages although the maximum amplitudes did vary. The flutter frequencies were nonengine order and varied from 9.47 to 9.91 engine orders. The effect of inlet pressure and temperatureson the flutter boundaries is shown in Figs. 15 and 16. As can be seen from these, increasing inlet pressure is, as usual, destabilizing. However, increasing inlet temperature was found to be stabilizing which is the inverse of the trend observed on the rotating stages. This type of trend is indicative of a density effect. The effect of inlet pressure and temperature on the flutter frequency is seen in Fig. 17. Here we see the usual trend due to increasing inlet pressure, a reduction in the flutter frequency. Increasing inlet temperature tended to also reduce the flutter frequency in much the same way as observed in the fan stall flutter data. Analysis of the stage aerodynamic data did not indicate choking, thus the instability is probably a form of stall flutter. Since this stator has a negative incidence angle at the tip the phenomena observed was probably negative incidence stall flutter.

Turbojet Engine - System Mode Instability

One of the principle priorities of the turbojet aeromechanical program was to thoroughly document a second rotor system mode instability that was known to exist on the engine model being tested. Unfortunately, the particular engine build used was not very sensitive to this instability and only one low stress level transient data point was obtained. However, some insight into this type of instability was obtained.

The system mode instability was first observed during the engine's development program and was resolved by closing the first stator to decrease the incidence on the second rotor. This instability is of interest because it is not commonly seen and thus not well understood. It occurred in the second system mode which involves a coupling of above shroud first bending and first torsion. Stress levels of the order of ±100 MPa (±14.5 ksi) were observed in the development program. The instability has two branches as seen in Fig. 18. In this program the lower branch was not found. The upper branch was found and at the time unknowingly transcended at 96 percent of physical design speed (82.7% corrected speed).

It was anticipated that some rather severe stress levels would occur once the instability boundary was penetrated. This did not occur. The instability was approached by doing a slow acceleration to 100 percent design speed with nominal inlet conditions of 200 kPa (29 psia) and 121° C (250° F). Near 96 percent physical speed a slight action on the strain gages was noted, less than ±30 MPa (±4.3 ksi). The excursion was slowed in anticipation of an instability. However, the strain gages quickly subsided and nothing more was noted for the remainder of the excursion. The recorded strain gage data was analyzed after the test run and it became apparent only then that the slight strain gage activity noted had indeed been an instability that had been transversed.

Analysis of the strain gage data indicated a nonintegral order response over a narrow speed range. The maximum stress level observed on any strain gage was ±24.8 MPa (±3.6 ksi) at 1370 Hz. This frequency is not a fundamental blade frequency but is associated with a second rotor system mode. An expanded spectrum plot of the maximum strain gage signal is shown in Fig. 19, which shows that the principal response of the strain gage is quite removed from an engine order response. A plot showing stress level and frequency versus physical engine speed is shown in Fig. 20. Prior to penetrating the instability there was only a slight nonintegral order response at 1374 Hz. At 95.9 percent physical speed the stress level began to rise and reached a maximum at 96 percent physical speed at a frequency of 1370 Hz. Shortly thereafter, the stress levels began to decrease and the frequency increase. At 97 percent physical speed the instability was cleared. The decrease in frequency noted in this data is probably due to increased damping as the stress amplitudes increased. This is simply described by the equation:

$$\omega_f = \omega_n(1 - \zeta^2)^{\frac{1}{2}} \qquad (5)$$

The damping coefficient ζ is sensitive to amplitude variations. The two most active strain gages were analyzed to determine their phase relationships. The phase angle between the two at the time of maximum stress was 3.07° which meant that they were nearly in phase.

To induce the instability it was necessary to open the first stator to increase the incidence angle of the second rotor and to also close the second stator to increase the stage pressure

ratio. In addition the variable geometry schedule was shifted to track, within limits, on the stall side of the schedule. Thus, the instability was induced much like a stall instability. It should be noted that there was no evidence of flow separation in any of the data.

The test conditions used to obtain this data were the extreme allowable maximum conditions thus it was not possible to further explore this instability without exceeding established safe engine practices.

Concluding Remarks

As was seen from the data presented several types of instabilities were investigated. It was found that each type had a unique set of characteristics that distinguished it from the others. The types of instabilities included two forms of subsonic stall flutter, choke flutter and a system mode instability. A comprehensive compilation of aerodynamic and aeromechanical data were obtained relevant to each type of instability. This data has been and is yet being analyzed by both the NASA and the various engine manufacturers involved in these programs.

The Joint Engine System Research aeromechanical programs are continuing with a number of programs planned for the future. Additional data will be collected relative to several types of aeroelastic instabilities. In addition, the scope of the aeromechanical programs has been expanded to acquire structural dynamic data relative to a wide variety of inlet distortion stimuli.

References

1. Adamczyk, J. J., "Analysis of Supersonic Stall Bending Flutter in Axial-Flow Compressor by Actuator Disk Theory," NASA TP-1345, 1978.
2. Carta, F. O., "Coupled Blade-Disk-Shroud Flutter Instabilities in Turbojet Engine Rotors," J Journal of Engineering for Power, Vol. 89, No. 3, July 1967, pp. 419-426.
3. Jones. W. H., Bishop, W. A., Kirchgessner, T. A., and Dicus, J. H., "Experimental Apparatus for Investigation of Fan Aeroelastic Instabilities in Turbomachinery," NASA TM X-3508, 1977.
4. Nieberding, W. C. and Pollack, J. L., Optical Detection of Blade Flutter," ASME Paper 77-GT-66, Mar. 1977.
5. Kurkov, A. and Diçus, J. H., "Synthesis of Blade Flutter Vibratory Patterns using Stationary Transducers," ASME Paper 78-GT-160, Apr. 1978.
6. Smalley, R. R., "Microprocessor Based Multichannel Flutter Monitor using Dynamic Strain Gage Signals," NASA TM X-71884, 1976.
7. Whitehead, D. S., "Torsional Flutter of Unstalled Cascaded Blades at Zero Deflection," ARCR & M 3429, 1964.
8. Den Hartog, J. P., Mechanical Vibrations, 4th ed. McGraw-Hill, New York, 1956, pp. 363-369.

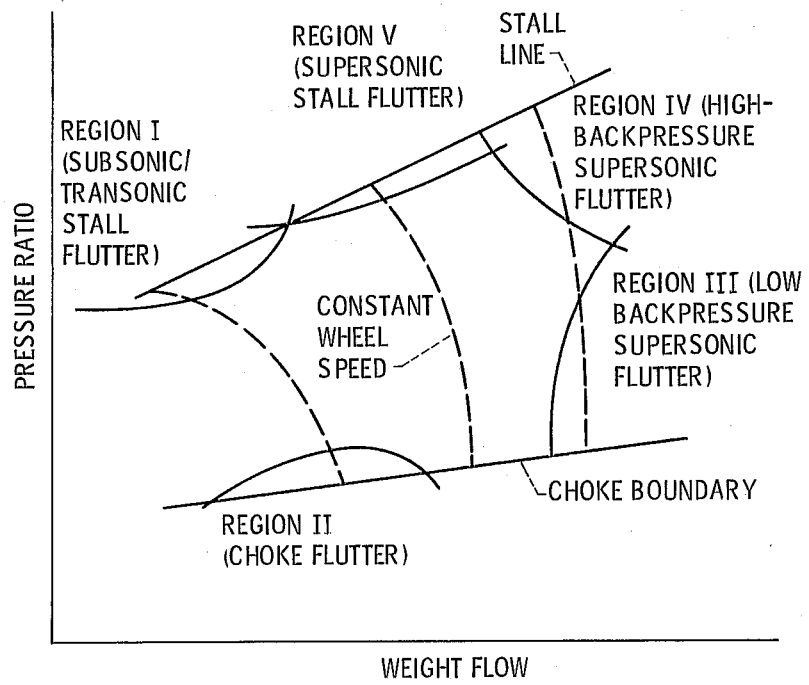

Figure 1. - Compressor performance and stability map.

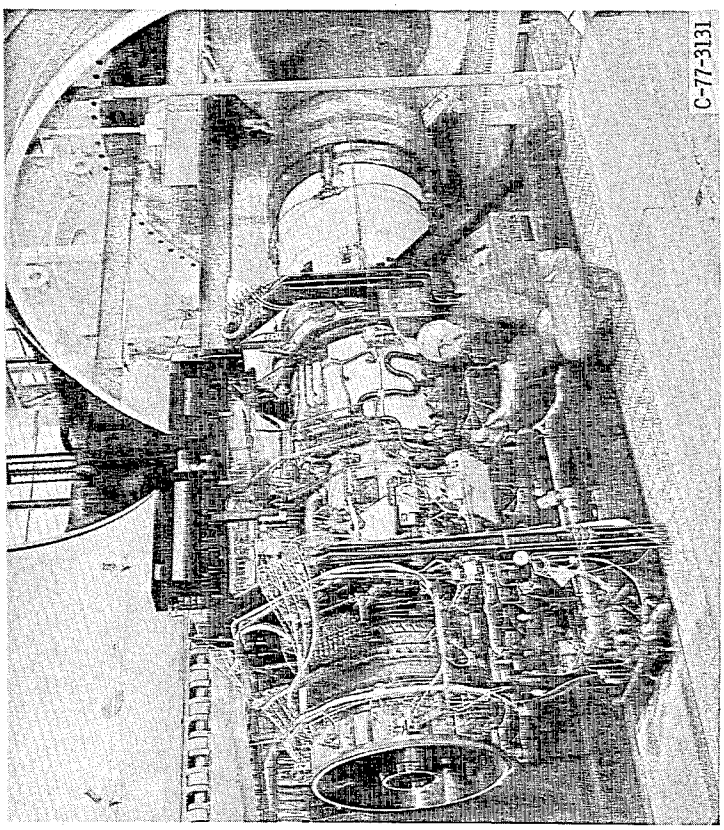

Figure 2. - Turbofan engine installation.

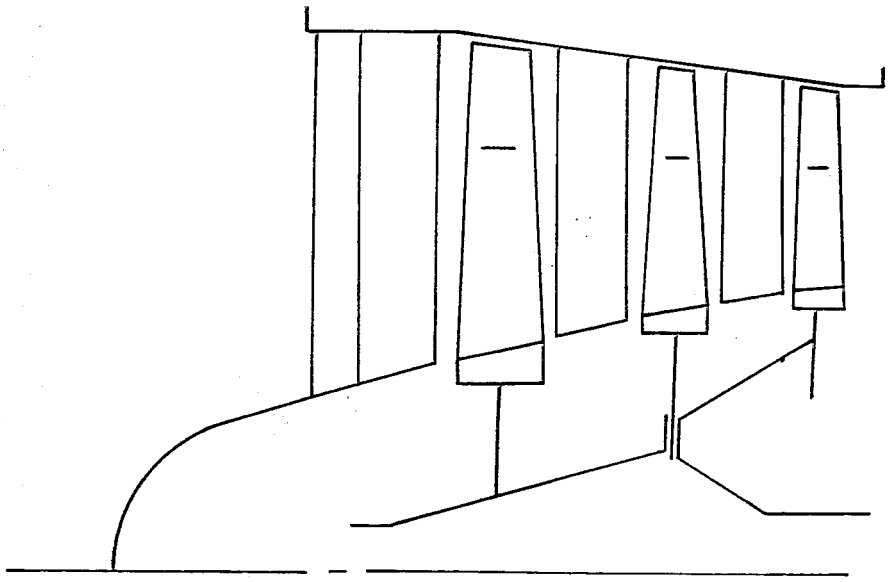

Figure 3. - Schematic of fan cross section.

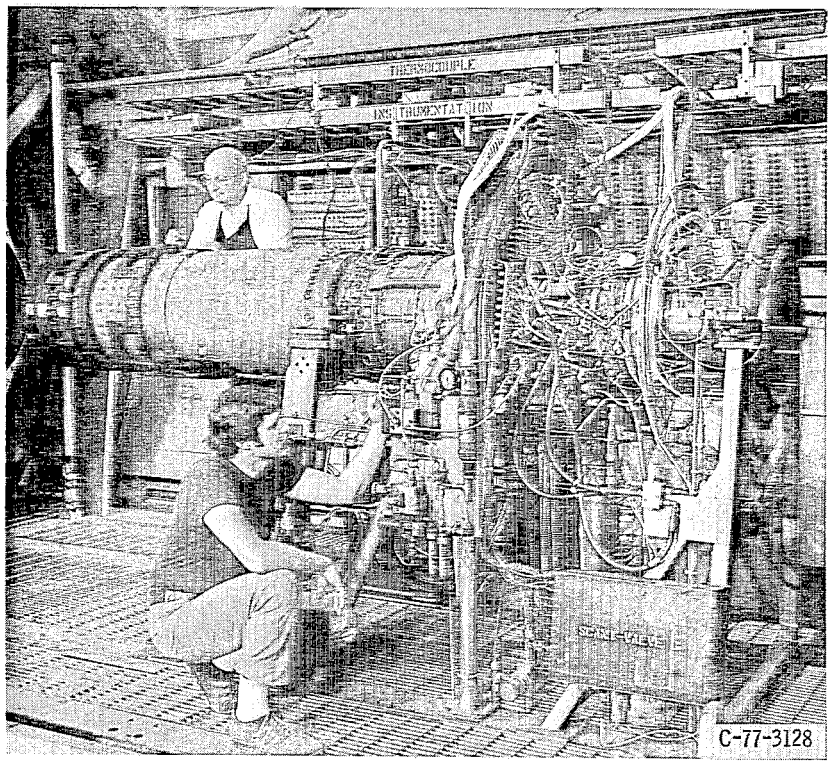

Figure 4. - Turbojet engine installation.

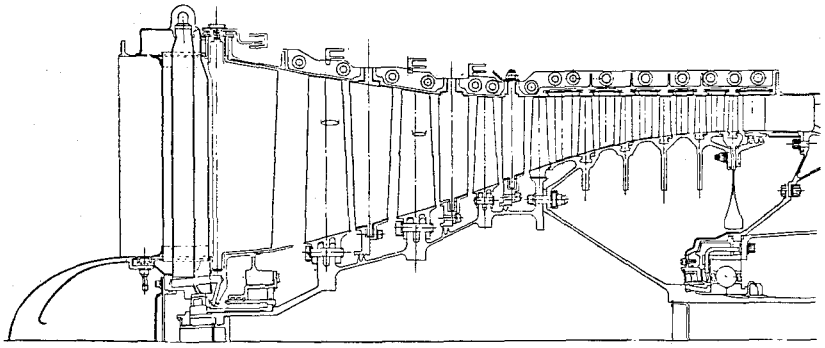

Figure 5. - Schematic of fan cross-section.

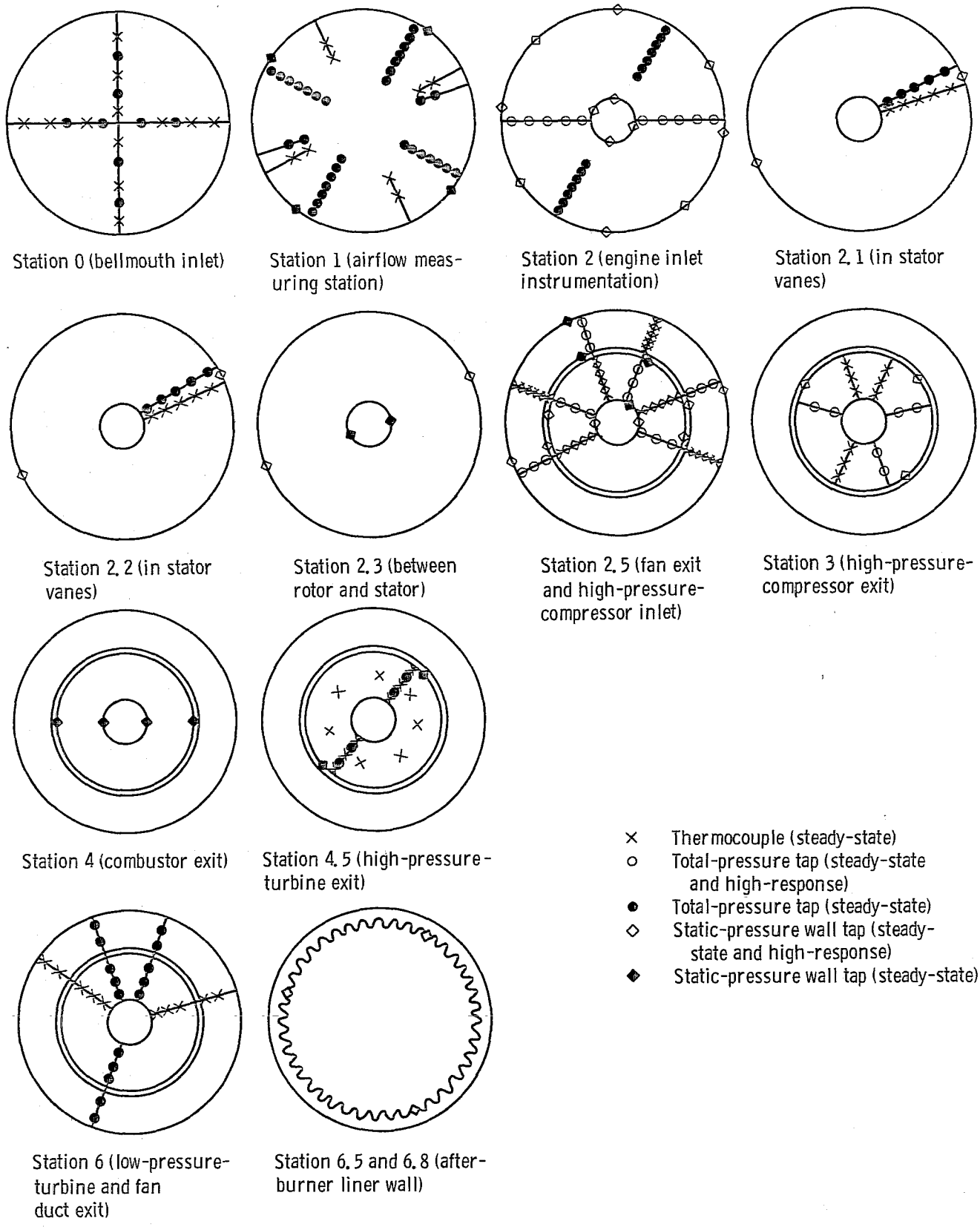

E-9208

Figure 6. - Schematic of aerodynamic instrumentation locations at each measuring station (viewed looking upstream).

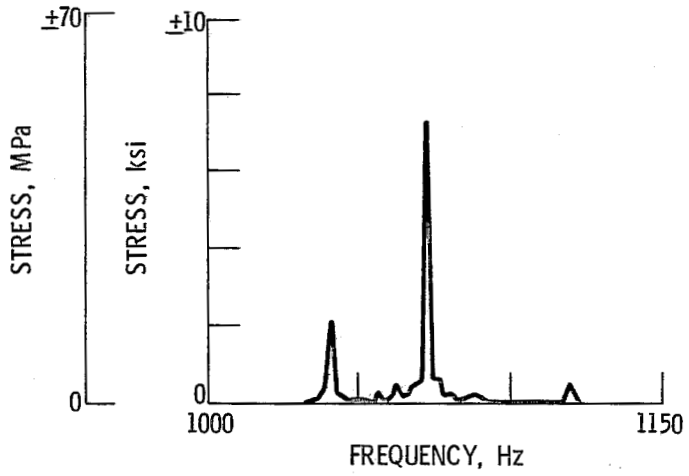

Figure 7. - Expanded spectrum plot of fan stall flutter at 172 kPa (25 psia) and 171^{0} C (340^{0} F).

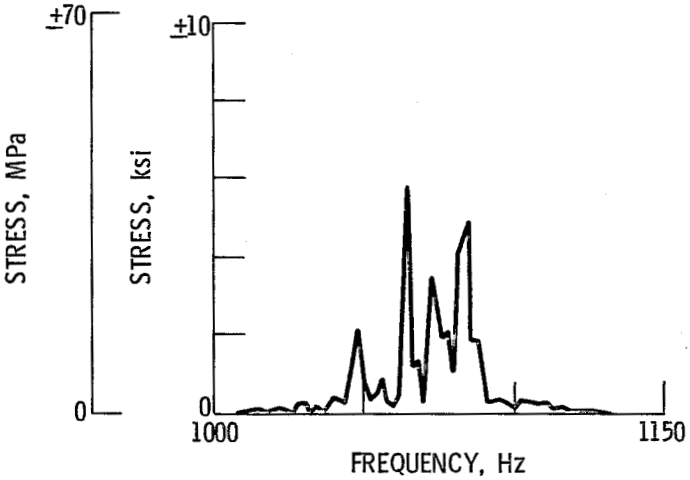

Figure 8. - Expanded spectrum plot of fan stall flutter at 172 kPa (25 psia) and 135^{0} C (275^{0} F).

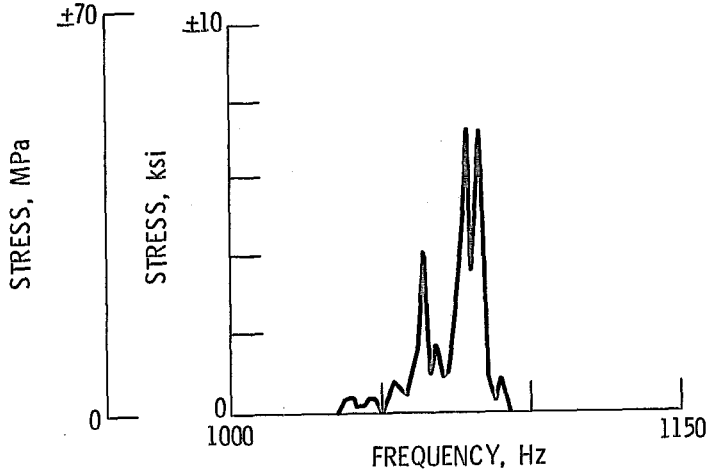

Figure 9. - Expanded spectrum plot of fan stall flutter at 172 kPa (25 psia) and 135° C (275° F).

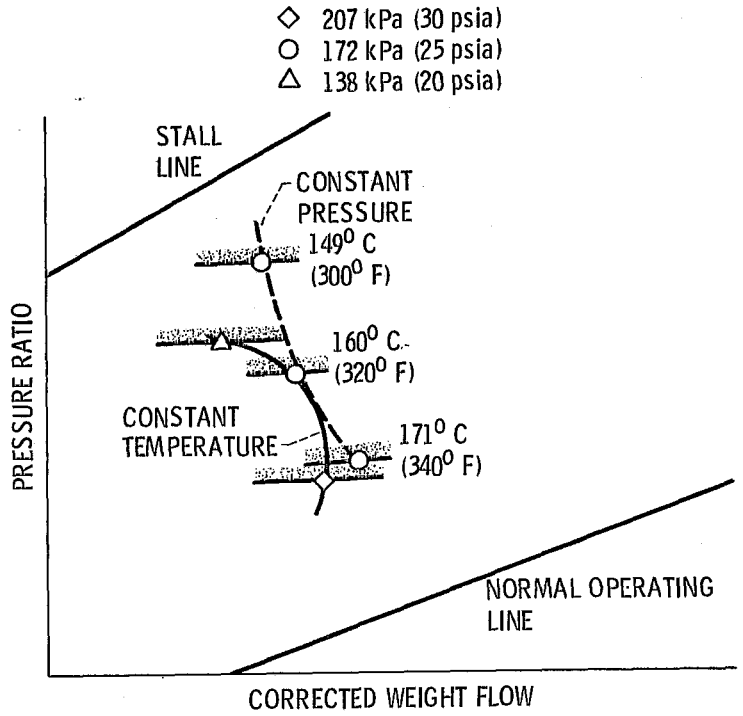

Figure 10. - Fan performance map showing inlet pressure and temperature effect on turbofan stall flutter boundary.

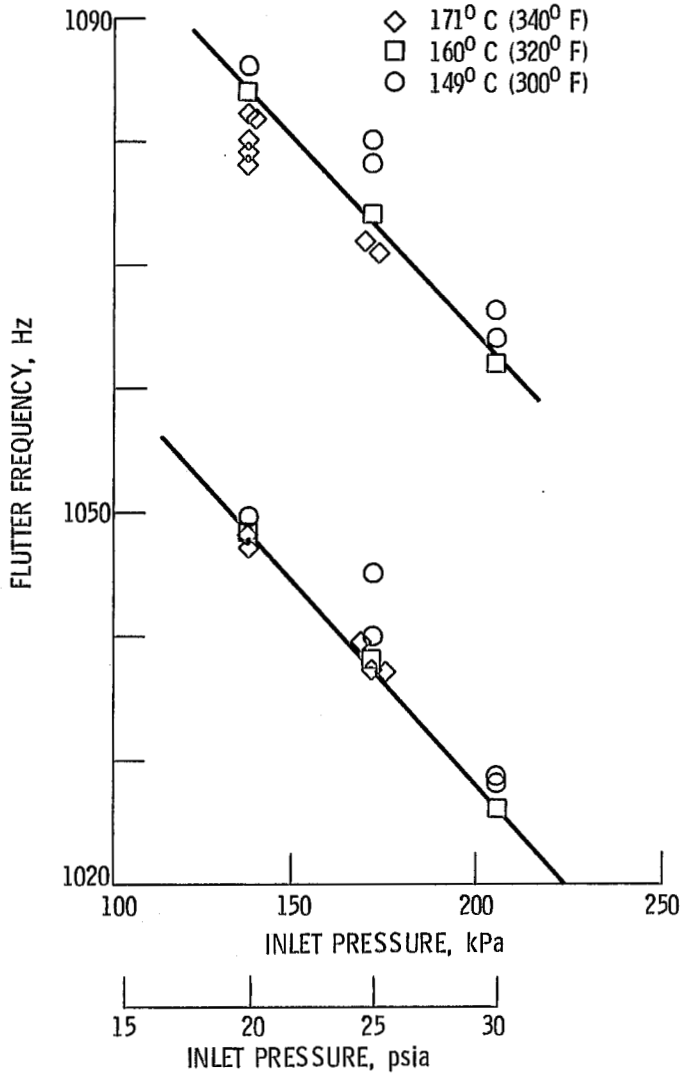

Figure 11. - Inlet pressure and temperature effect on fan stall flutter frequency.

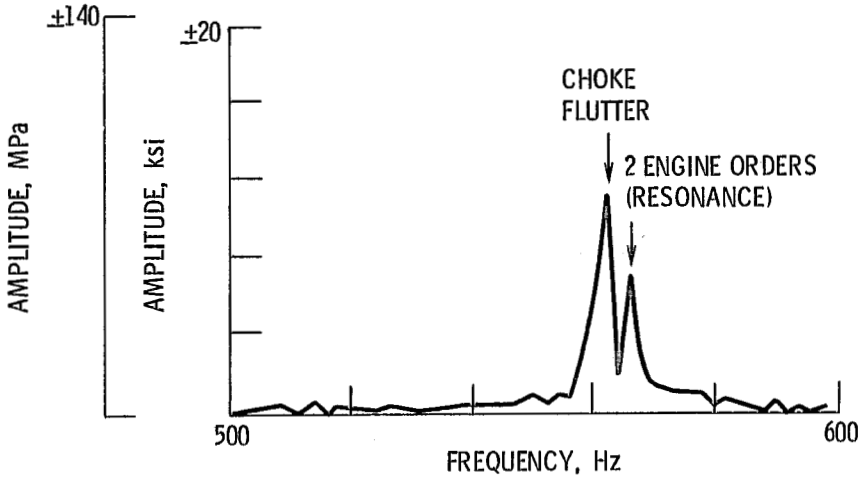

Figure 12. - Choke flutter strain gage spectrum.

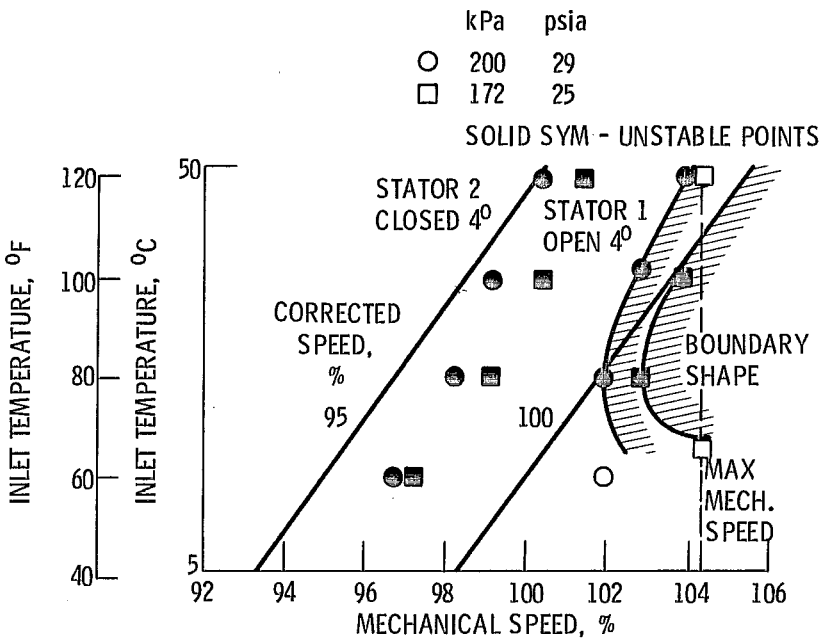

Figure 13. - Choke flutter boundaries as a function of inlet temperature and engine speed.

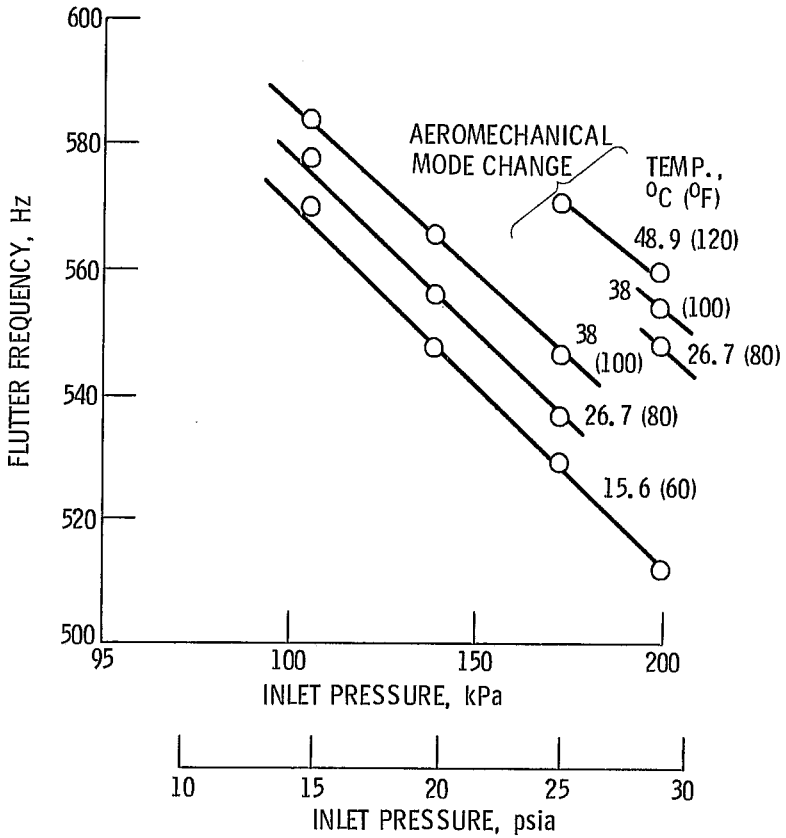

Figure 14. - Effect of inlet pressure and temperature on third rotor choke flutter.

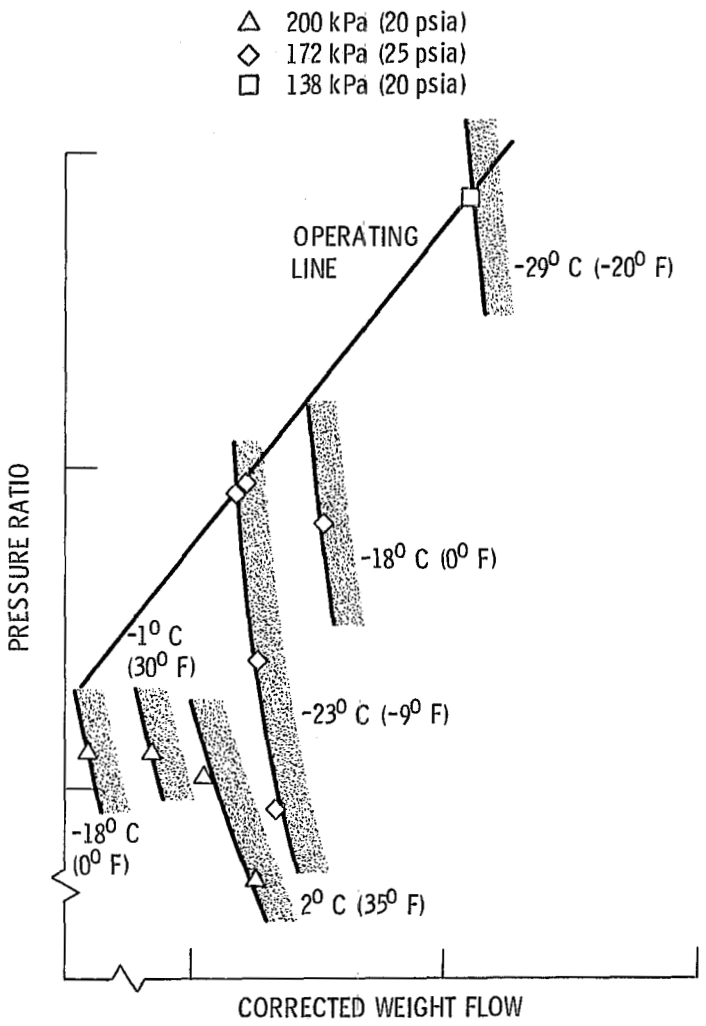

Figure 15. - Compressor performance map showing inlet pressure and temperature effects on fourth stator instability boundaries.

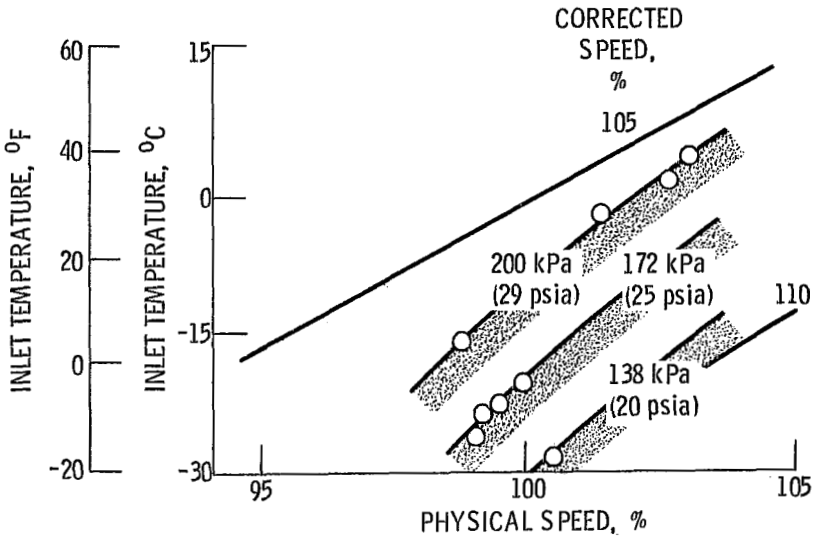

Figure 16. - Fourth stator instability boundaries as a function of inlet pressure, inlet temperature, physical speed and corrected speed.

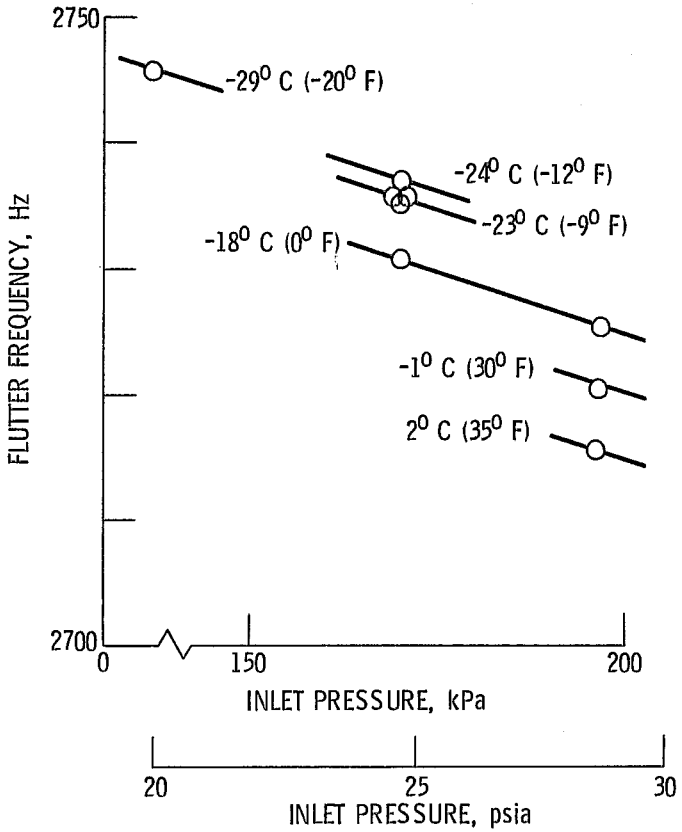

Figure 17. - Effect of inlet temperature and pressure on fourth stator flutter frequency.

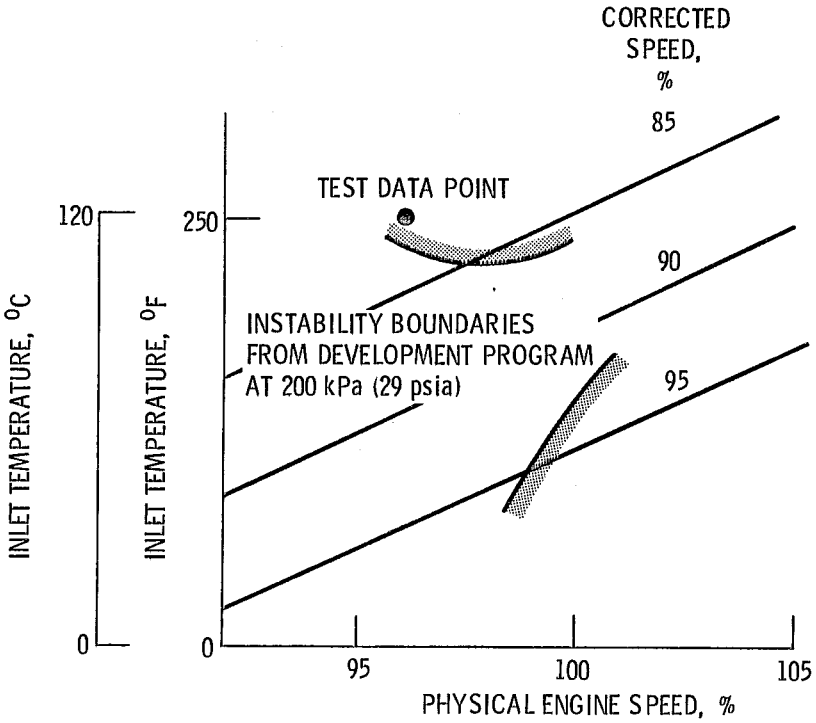

Figure 18. - System mode instability boundaries as a function of inlet temperature and engine speed.

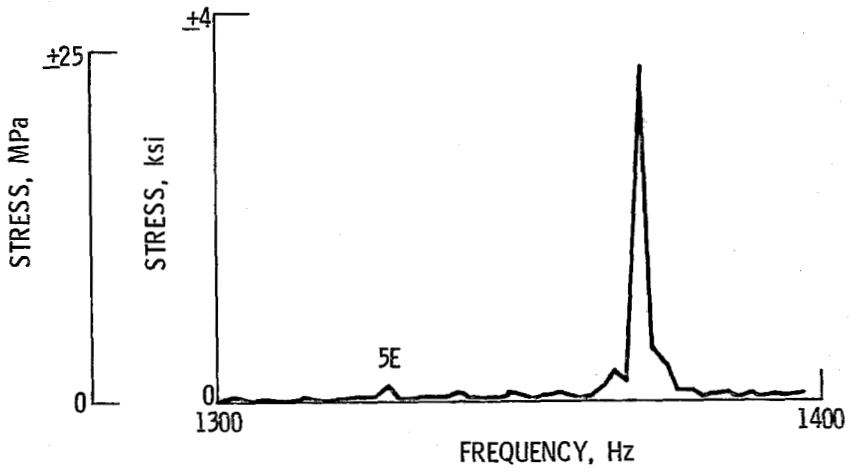

Figure 19. - Expanded spectrum plot of system mode instability.

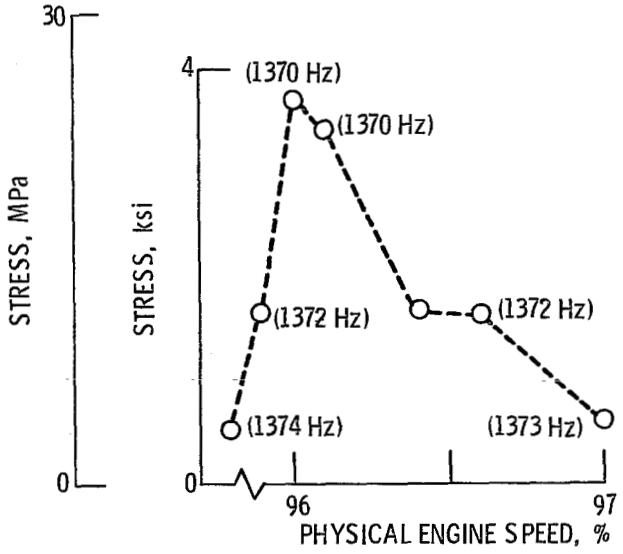

Figure 20. - System mode instability stress and frequency as a function of engine speed.

Page Intentionally Left Blank